Supplementary Information

Mid-Pliocene warm-period deposits in the High Arctic yield insight into camel evolution

Natalia Rybczynski[1]*, John C. Gosse[2*], C. Richard Harington[1], Roy A. Wogelius[3], Alan J. Hidy[2], Mike Buckley[4]*

[1]Palaeobiology, Canadian Museum of Nature, Ottawa, Ontario, K1P 6P4, Canada, [2]Department of Earth Sciences, Dalhousie University, Halifax, Nova Scotia, B3H 4R2, Canada, [3]SEAES, Williamson Building, Oxford Road, University of Manchester, Manchester M13 9PL, UK, [4]Manchester Institute of Biotechnology, University of Manchester a, 131 Princess Street, Manchester, M1 7DN, UK.

*To whom correspondence should be addressed.
E-mail: nrybczynski@mus-nature.ca; john.gosse@dal.ca; m.buckley@manchester.ac.uk

Contents

Part 1. Supplementary Figures S1-S5

Supplementary Figure S1

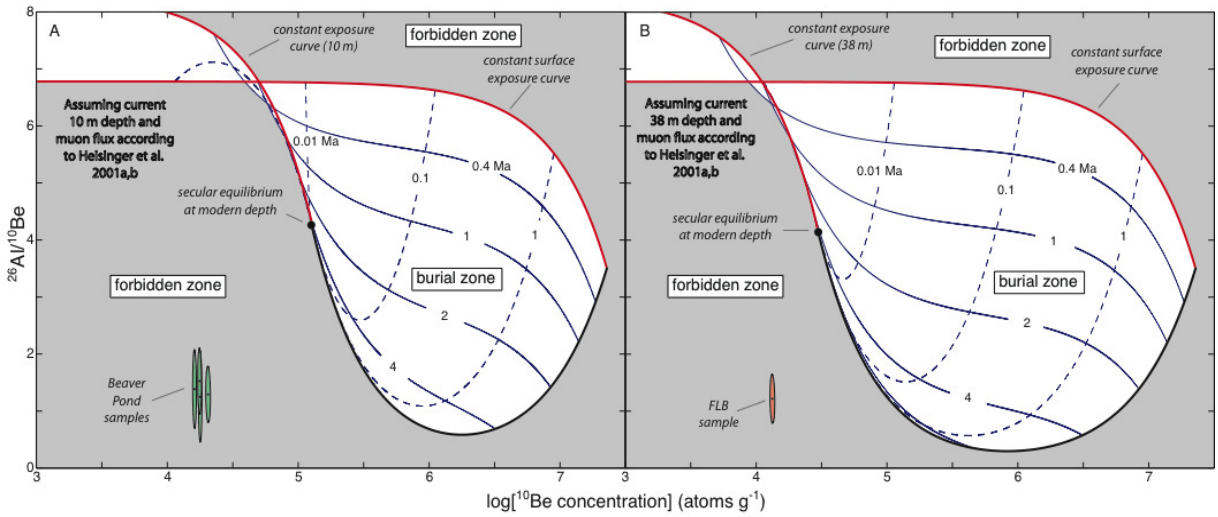

$^{26}Al/^{10}Be$ *vs* log^{10}Be plots assuming that the sample depths have been constant with time and assuming post-depositional muon production based on modern sample depths. Samples at the two sites (**A**: Beaver Pond site; **B**: Fyles Leaf Beds site) are plotted on different graphs because of the depth difference between the two sites, which changes muonic production and thus the shape of the graph. Muonic production as per Heisinger *et al* [45,46]. The shaded areas represent forbidden regions where samples should not plot given a simple burial model that includes muon production rates at 10 m and 38 m for the Beaver Pond and Fyles Leaf Beds sites, respectively. A sample plotting in the forbidden zone and beneath the secular equilibrium line indicates an overestimate of the muon production rate and therefore and underestimate in the time-averaged sample depth.

Supplementary Figure S2

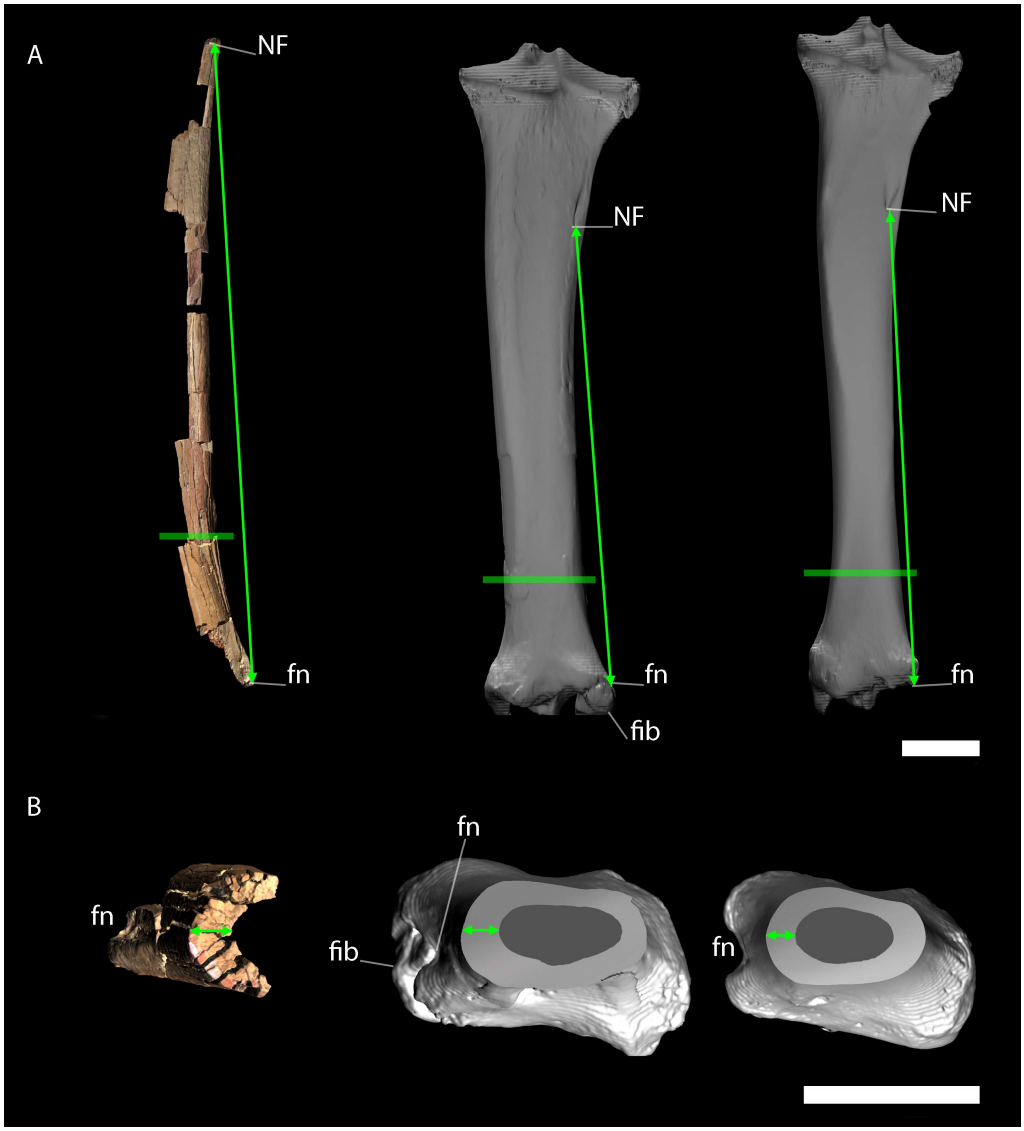

Comparison of camel tibiae specimens. From left to right: Ellesmere camel (NUFV 210), *Camelus bactrianus* (CMNMA 32202), *Camelus dromedarius* (ROM MAM 94191). **A**, right tibiae in posterior view, with green arrows showing length measurements between fibular notch and nutrient foramen. **B**, cross sectional views of distal end of tibial shafts, with green arrows to show cortical thickness measurements. The horizontal green lines in part A show location for cross-sectional views in B. NUFV 210 specimen image was generated from surface scans collected using an Arius 3-D laser scanner, and processed using Pointstream 3DImageSuite (CMN, Arius 3D center). The CT images were rendered in Avizo, and measured in 3D StudioMax (CMN, Arius 3D center). Institutional abbreviations: **CMNMA**, Canadian Museum of Nature, Mammal collections; **ROM MAM**, Royal Ontario Museum, Mammal collections. Anatomical abbreviations: **Fib**, Fibula; **fn**, fibular notch; **NF**, Nutrient foramen. Scale bar, 5 cm.

Supplementary Figure S3

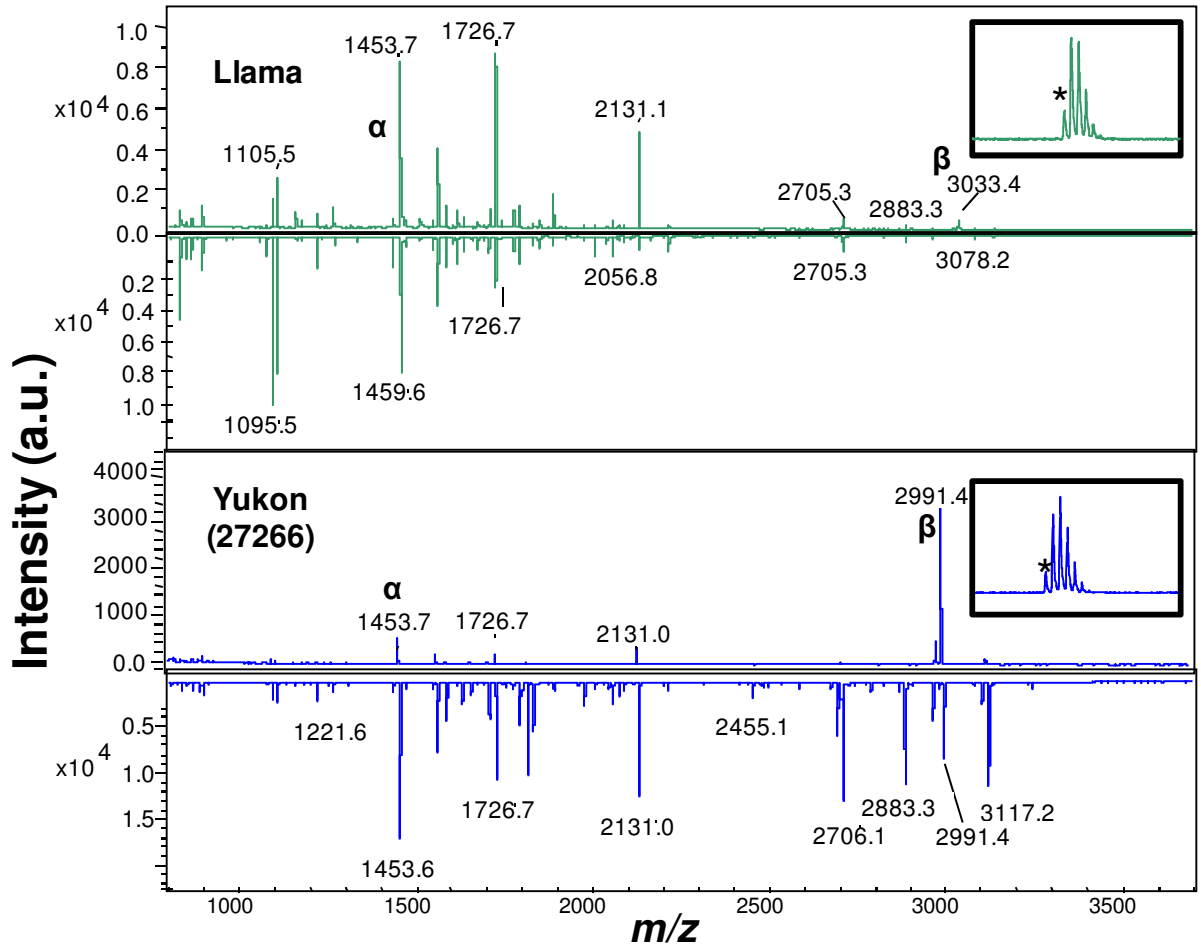

MALDI-ToF-MS spectra of collagen digests from a Yukon fossil specimen and *Lama glama* specimen. 'α' denotes homologous peptides (see **Supplementary Fig. S4**) showing species-specificity between the two extant camel species; 'β' denotes one of the most intense species markers observed at *m/z* 2992 (see **Supplementary Fig. S5**) representing the peptide sequence GPSGEAGTAGPPGTPGPQGLLGAPGFLGLPGSR, where P = Hyp and the Q represents a deamidated glutamine) described previously[24]. Insets show the isotopic envelopes for peptide 'β' (with the monoisotopic peak marked with an asterix), within which the effect of increased Q deamidation in the ancient peptides (e.g., from the Yukon sample, CMN 27266) can be observed.

Supplementary Figure S4

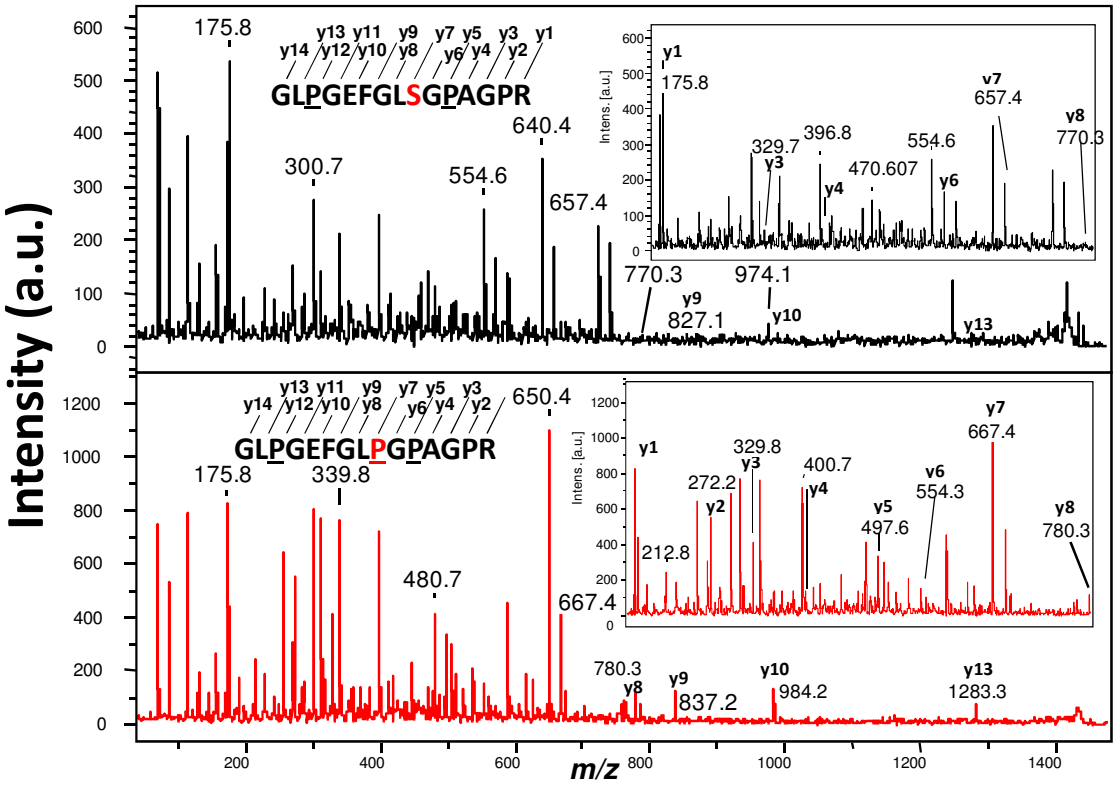

Tandem MALDI-ToF-MS spectra that show the sequencing of two homologous peptides found in camelid type 1 collagen at *m/z* 1453 and *m/z* 1443. Sequencing confirms that these peaks represent peptide sequences GLPGEFGLPGPAGPR for the peptide *m/z* 1453 and GLPGEFGLSGPAGPR for the peptide *m/z* 1443, where P represents hydroxylated proline residues. The predominant y-ion series, the C-terminus containing fragment ions that occur at C-N bond cleavage, is shown to be similar in both peptide analyses amongst a large number of internal fragments. The amino acid substitution can be observed to occur at the 9th amino acid, a 10 Th shift that indicates a shift from the Proline to a Serine residue. Inset shows a close up of the region *m/z* 150-800. Labelling of fragment ions follows Roepstorff & Fohlman[47].

Supplementary Figure S5

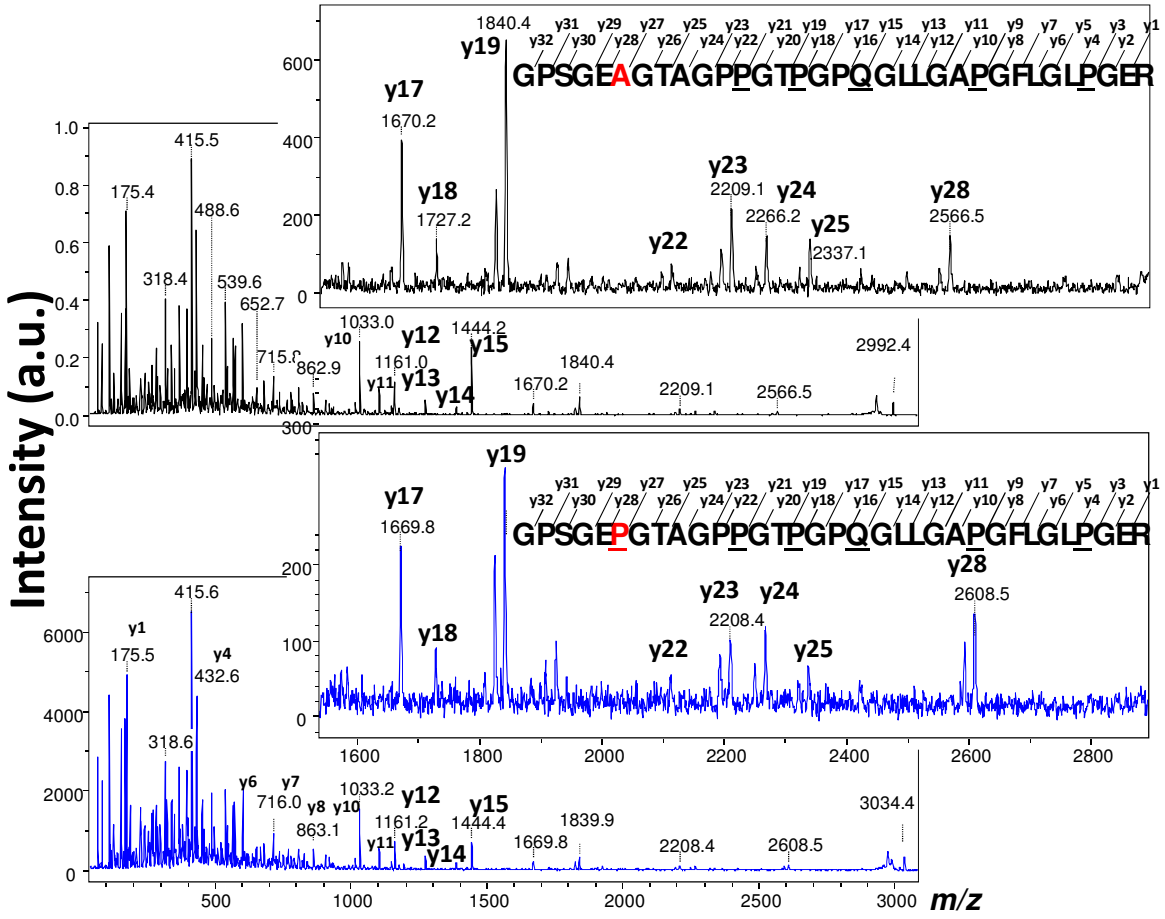

Tandem MALDI mass spectra of the deamidated Camelini-specific peptide marker at *m/z* 2992 in comparison to the homologous peptide in Lamini at *m/z* 3034; P = Hydroxylated proline residue and Q = deamidated glutamine residue). Note that the single amino acid substitution, highlighted in red font, P->A affects a site that is normally hydroxylated. Inset shows a close up of the region *m/z* 1600-2800. Labelling of fragment ions follows Roepstorff & Fohlman[47].

Part 2. Supplementary Tables S1-S4

Supplementary Table S1. Measurements for estimating original tibia length of NUFV 210. Measurements in mm.

Taxon	Catalogue number	Distance between fibular notch and nutrient foramen*	Cortical thickness*	Tibia length
Camelus bactrianus	CMNMA 5657	296.0	8.7	441.8
C. dromedarius	ROM MA 94191	304.6	8.4	450.2
Ellesmere camel	NUFV 210	(389.3)**	12.0	?

* See **Supplementary Fig. S1** for illustration of measurements.

** This is a minimum estimate. See methods section in main text.

Supplementary Table S2. Comparisons of some dental and postcranial measurements of North American and Eurasian giant camels. Measurements are in millimeters.

Taxon	Age	Distribution	Second lower molar length	Proximal phalanx length	Tibia length
Megacamelus	L. Miocene – E. Pliocene	North America (USA)	48 - 55[1]	124.1 ± 8.4[7]	670[7]
Megatylopus	M. Miocene– E. Pliocene	North America (USA)	39 – 50[1]	?	~620[e]
Ellesmere camel (NUFV 210)	Pliocene	North America (Arctic)	?	?	~575 (estimation)
Yukon cf. *Paracamelus*	Pleistocene	North America (Arctic)	46.8[a]	123.8 ± 8.0[b]	?
Paracamelus gigas	Pliocene	Eurasia (Asia)	44[48]	Forelimb: 130 Hind limb: 121[48]	600[48]
P. cf. aguirrei	L. Miocene	Eurasia (Europe)	43.7[49]	?	?
Camelus knoblochi	Middle-Late Pleistocene	Eurasia	43.0, 49.2[50]	?	?
C. bactrianus	Extant	Native to Eurasia	33.5 - 43.0[49]	Forelimb: 100 Hind limb: 91[c]	442[c]
C. dromedarius	Extant	Native to Arabia	38.5[51]	Forelimb: 100 Hind limb: 88[d]	450[f]

[a]CMN 47917; [b]CMN 27266, 26957, 14775, 8623; [c]CMNMA 32202; [d]CMNMA 44002; [e]AMNH 20479; [f]ROM MAM 94191.

Abbreviations**: AMNH**, American Museum of Natural History; **CMN**, Canadian Museum of Nature; **CMNMA**, Canadian Museum of Nature, Mammal collections; **ROM MAM**, Royal Ontario Museum Mammal collections.

Supplementary Table S3. Sample thickness averaged 5 cm for all sediment samples. Site latitude and longitude for Beaver Pond (BP) Site (402 m asl) and Fyles Leaf Bed (FLB) Site (358 m asl) are approximately 78.55 N and 82.50 W. Exact locations are not provided to help preserve the fossil sites, and can be requested from the first author. All AMS (Accelerator mass spectrometry) measurements are from Lawrence Livermore National Laboratory. SF-08-C-016 yielded insufficient ^{26}Al current, and SF-08-C-17 yielded an ICP-MS Al concentration that failed gravimetric verification based on the mass of Al standard added as carrier. Granitic boulder SF-08-C-014 attributes: location: 78.541817N, 82.339833W, 431 m; sample thickness: 6 cm (chiselled); 60 cm height.

Field ID	CNEF ID	Be AMS ID	Al AMS ID	Density	^{10}Be in quartz		^{27}Al in quartz		^{26}Al in quartz		^{26}Al/^{10}Be	
				(g/cm3)	Conc. (atom/g) x 10^3	Unc 1σ	Conc. µg/g	Unc 1σ	Conc. (atom/g) x 10^3	Unc 1σ	Ratio atom/atom	Unc 1σ %
BP Site												
SF-08-C-001	JG 2151	BE26332	AL12131	2	20.51	0.60	260.8	13.0	26.47	7.14	1.29	27.6%
SF-08-C-002	JG 2152	BE26333	AL12132	2	17.85	0.39	274.0	13.7	22.28	10.20	1.25	46.1%
SF-08-C-003	JG 2153	BE26334	AL12133	2	16.16	0.38	296.0	14.8	22.37	7.93	1.38	35.9%
SF-08-C-004	JG 2154	BE26335	AL12134	2	17.66	0.40	247.6	12.4	26.94	7.32	1.53	27.8%
FLB Site												
SF-08-C-015	JG 2157	BE26336	AL12135	1.9	13.32	0.40	127.4	6.4	16.20	4.06	1.22	25.8%
SF-08-C-016	JG 2158	BE26337	AL12136	1.9	11.54	0.30	93.8	4.7	3.29	3.05	0.28	93.1%
SF-08-C-017	JG 2159	BE26338	AL12137	1.8	14.69	0.59	67.3	3.3	8.99	2.34	0.61	26.9%
Boulder												
SF-08-C-014	JG2156	BE27611		2.6	554.1	11.58						

Field ID	Quartz Mass (g)	Be Carrier Mass (g)	^{10}Be/^{9}Be corr	^{10}Be/^{9}Be unc (1σ AMS)	Al Carrier Mass (g)	^{26}Al/^{27}Al corr	^{26}Al/^{27}Al unc (1σ AMS)
SF-08-C-001	150.0295	0.1990	2.51E-13	7.32E-15	0.8723	4.96E-15	1.34E-15
SF-08-C-002	150.1458	0.2042	2.15E-13	4.66E-15	0.8668	3.96E-15	1.81E-15
SF-08-C-003	120.701	0.2073	1.58E-13	3.67E-15	1.2846	3.65E-15	1.29E-15
SF-08-C-004	150.0137	0.2034	2.13E-13	4.86E-15	0.8625	5.30E-15	1.44E-15
SF-08-C-015	150.2456	0.2047	1.63E-13	4.94E-15	0.8688	6.17E-15	1.55E-15
SF-08-C-016	150.8411	0.2071	1.42E-13	3.73E-15	0.8645	1.78E-15	1.65E-15
SF-08-C-017	150.6993	0.2049	1.79E-13	7.23E-15	0.8701	6.29E-15	1.64E-15
SF-08-C-014	91.8585	0.2222	3.54E-12	7.40E-14			

Supplementary Table S4. Burial ages.

Field ID	$^{26}Al/^{10}Be$		Burial age		Site
	atom/atom	% (1σ)	**Ma**	+/- (1σ)	
SF-08-C-001	1.29	29%	3.5	1.1/0.7	BP
SF-08-C-002	1.25	47%	3.6	2.2/1.1	BP
SF-08-C-003	1.41	37%	3.4	1.5/0.9	BP
SF-08-C-004	1.53	29%	3.2	1.1/0.7	BP
	error weighted mean:		**3.4**	**0.6/0.4**	
SF-08-C-015	1.22	27%	3.7	1.0/0.7	FLB
SF-08-C-016	*0.29*	*94%*	*No age*		
SF-08-C-017	*0.61*	*28%*	*No age*		

Part 3. Supplementary Methods

3.1 Geochronology

The premise of burial dating is that ^{10}Be and ^{26}Al is produced in a mineral exposed to cosmic ray secondaries (primarily fast neutrons and muons) in the upper few metres of Earth's surface until it becomes buried under many metres of sediment, glacier ice, or other material, at which time there is little or no cosmogenic production of the isotopes. The production ratio of ^{26}Al/^{10}Be at the Earth-Atmosphere interface is relatively well known (6.75 at the surface, sea level, high latitude using the standards KNSDT10650 for ^{26}Al and 07KNSTD3110 for ^{10}Be). The ratio changes (mostly decreases) after burial because the half life of ^{26}Al (0.72 Ma) is shorter than ^{10}Be (1.38 Ma). However, the ratio also changes with depth because production near the surface is mostly due to spallation, whereas at depths greater than about 4 m of rock the production ratio is greater due to the greater propensity to produce muogenic ^{26}Al relative to ^{10}Be. This complication, recognized after experiments on muon production by Heisinger et al. [45,46], results in a more complex depth-dependent computation of burial ages, unique for each sample depth.

We use the production rate calculations by Balco et al. [52] for a surface rate (at ~400 m) but assume a longer term average rate scaled from sea level using Lal [53] as modified by Stone [54]. For instance, using the current version of the calculator (V. 2.1), at the top of the BP section (402 m) the spallogenic and muonic production rate in quartz of ^{10}Be is 6.95 and 0.211 atoms g^{-1} yr^{-1} and ^{26}Al is 46.88 and 1.759 atoms g^{-1} yr^{-1}. For all samples at the BP and FLB sites we believe there is a negligible muonic component because (i) part of the section was eroded by the overriding glaciers during many of the >20 glaciations over the past 2.95 Ma, and (ii) equivalents of the Innuitian ice sheet would have persisted in the area for much of that time, therefore adding additional shielding (even today the margin of a large ice cap persists at a similar elevation approximately 30 km to the northeast). Thus, the modern measured mass-depths for the burial age samples should be considered only minimum values, and are likely significantly less than the time-averaged mean value. In support of our assumption of negligible muonic production, when the samples are plotted on a ^{26}Al/^{10}Be -^{10}Be burial plot, they fall in a forbidden zone outside the limits of exposure and burial duration boundaries if muonic production as described by Heisinger et al. is considered using modern mass-depths **(Fig. S2).** However, if little or no muonic contribution is considered, as would be expected if the sites experienced a much greater time-averaged mass-depth, the samples fall within the burial field of the plot. Although the measured ^{10}Be and ^{26}Al concentrations include some post-depositional production by muons, without knowledge of the mass-depth history of the samples quantifying the muonic component is unfeasible. Thus the burial ages described in the text are considered <u>minimum</u> ages. We also assume negligible tectonic or isostatic surface uplift over the entire burial duration. The actual integrated pre-burial and syn-burial muonic production rates may be a little lower if surface uplift occurred, however this will have a negligible effect on the ^{26}Al/^{10}Be production ratio, which is used for burial dating.

We also considered the possibility that the initial $^{26}Al/^{10}Be$ prior to final deposition was not 6.75. The ratio will be less if the quartz sand experienced previous prolong (i.e. > 200 ka) burial episodes prior to this final deposition. However, this is unlikely at this location. The catchment source area is higher than the high terrace gravel deposits. The fauna and flora, palaeo-thermometry, and lack of glacial sediments below the peats, all suggest that the sediments were deposited prior to the Late-Pliocene and Quaternary glaciations, and therefore were not shielded under thick ice for a prolonged time prior to deposition. The reproducibility (coefficient of variation of 4.8%) of the four ages at the BP site and close agreement of the other age at the FLB site suggest that if there were deviations from an initial ratio of 6.75, they were small. Thus, unlike many $^{26}Al/^{10}Be$ burial dating experiments which are interpreted to be maxima ages (i.e. if the initial ratio was < 6.75 the calculated age would therefore be an overestimate), we argue that the calculated ages at the FLB and BP site are probably within their total error indicated. Because the burial ages at this depth are more sensitive to post-depositional muonic production than a depressed initial ratio, we conservatively assume the burial ages are minima. The error-weighted mean values and uncertainties have been calculated using the linear variance method of Barlow (2004 web-based calculator) .[55]

The SF-08-C-014 boulder age is 78.9 ± 7.0 ka (1σ external error, including production rate uncertainty), as calculated using the Balco et al. [52] online CRONUS-Calculator version 2.1, with a time-varying production rate scaled by Lal [53] and Stone [54]. Although there was negligible evidence for boulder erosion, the boulder itself may have been exhumed from the till. Furthermore, the Eureka Weather Station, situated at sea level just 180 km NNW, receives between 6 and 27 cm of monthly snowfall, so it is likely that the surface of the high terrace gravel received a greater accumulation. The total effect of snow shielding depends too greatly on snow cover density, thickness, and duration to accurately estimate. However, both exhumation and snow cover will result in a measured age that underestimates the true age of the till surface, providing only a minimum limiting age, assuming negligible inheritance.

3.2 Collagen analysis

The 37 terrestrial mammal species initially available as standards (from Buckley[25,56-58]) are as follows:

Artiodactyla (17 species): cow (*Bos taurus*), pig (*Sus scrofa*), goat (*Capra hircus*), water buffalo (*Bubalus bubalis*), reindeer (*Rangifer tarandus*), red deer (*Cervus elaphus*), roe deer (*Capreolus capreolus*), fallow deer (*Dama dama*), bison (*Bison sp.*), hippopotamus (*Hippopotamus amphibius*), elk (*Alces alces*), saiga (*Saiga tatarica*), musk ox (*Ovibos moschatus*), dromedary camel (*Camelus dromedarius*), vicuna (*Vicugna vicugna*), pygmy hippopotamus (*Choeropsis liberiensis*), and sheep (*Ovis aries*).

Carnivora (9 species): brown bear (*Ursus arctos*), lion (*Panthera leo*), lynx (*Lynx lynx*), spotted hyeana (*Crocutta crocutta*), European badger (*Meles meles*), cat (*Felis sylvestris*), dog (*Canis lupus*), red fox (*Vulpes vulpes*) and Arctic fox (*Alopex lagopus*).

Lagomorpha (2 species): rabbit (*Oryctolagus cuniculus*), European hare (*Lepus europaeus*).

Perissodactyla (3 species): black rhinoceros (*Diceros bicornis*), Sumatran rhinoceros (*Dicerorhinus sumatrensis*), and horse (*Equus caballus*).
Rodentia (2 species): mouse (*Mus musculus*) and brown rat (*Rattus norvegicus*).
Proboscidea (4 species): African elephant (*Loxodonta africana*), Asian elephant (*Elephas maximus*), woolly mammoth (*Mammuthus primigenius*) and American mastodon (*Mammut americanum*).

Following closest matches of the FLB fragments to dromedary camel, collagen from the additional camelid specimens were also analysed following Buckley et al.[24], and are listed below. Abbreviations: AMNH, American Museum of Natural History; CMNMA, Canadian Museum of Nature, Mammal collections; ELMMZ, European Land Mammal Mega Zones; NALMA, North American Land Mammal Age; UNSM, University of Nebraska State Museum.

Modern taxa

Camelus bactrianus: CMNMA 32202

Vicugna pacos: CMNMA 32200

Lama glama: CMNMA 32201

Additional fossil taxa

Gigantocamelus spatulus: AMNH 24900 – fragment from Keim Formation, *Stegomastodon* Quarry, Brown Co. Nebraska, USA (NALMA Age, L. Blancan).

Megatylopus gigas: AMNH 41556-3 – Proximal phalanx from Snake Creek Formation, Sioux Co, Nebraska, USA (NALMA Age, Clarendonian-Hemphillian).

Paracamelus sp.: AMNH 19188 – Calcaneum from Tsagan Nor basin, Obor Hangay Province, C. Mongolia (ELMMZ, E. Villafranchian).

cf. Paracamelus (Yukon camel): CMN 27266 – proximal phalanx from Old Crow River Locality 29, Yukon, Canada (Plio-Pleistocene); CMN 48096 – distal fragment of metapodial from Old Crow River Locality 11A, Yukon, Canada (Plio-Pleistocene).

Titanotylopus nebraskensis: UNSM 91467 – fragment from distal left humerus from Loc Wt-15 Type locality, Nebraska, USA (NALMA Age, Irvingtonian).

A Fisher's Exact Test on the presence or absence of the one camelid marker, which we propose as being unique to the genus *Camelus* produces a significance value $p = 0.02632$ at a 95% confidence level (occurs once in 37 genera originally tested, excludes *Lama*; $p = 0.02564$ when *Lama* included). When this is extended to include further markers (e.g., the presence/absence of the two peptide markers at *m/z* 1453 and 2991 (α & β in **Fig. 4** & **Fig. S3**) 'species-specificity' is obtained in this particular set of data ($p = 0.02439$; occurs once in 40 species tested).

Lamini could be separated from Camelini using the peptide markers reported in Buckley *et al.*[25], including the additional llama and alpaca sampled in this study (e.g., **Fig. S3,** peak β**; Fig. S5**). Both Yukon fossils, CMN 27266 and CMN 48096 gave almost identical peak masses (*m/z* values) (compare **Fig. 4** with **Fig. S3**).

Part 4. Supplementary References

45 Heisinger, B. *et al.* Production of selected cosmogenic radionuclides by muons: 2. Capture of negative muons. *Earth and Planetary Science Letters* **200**, 357-369 (2002).

46 Heisinger, B. *et al.* Production of selected cosmogenic radionuclides by muons 1. Fast muons. *Earth and Planetary Science Letters* **200**, 345-355, doi:10.1016/s0012-821x(02)00640-4 (2002).

47 Roepstorff, P. & Fohlman, J. Proposal for a common nomenclature for sequence ions in mass spectra of peptides. *Biomedical mass spectrometry* **11**, 601 (1984).

48 Zdansky, O. *Paracamelus gigas*, Schlosser. *Paleontological Sinica* **2**, 1-44 (1926).

49 Titov, V. V. & Logvynenko, V. N. Early *Paracamelus* (Mammalia, Tylopoda) in Eastern Europe. *Acta Zoologica Cracoviensia* **49A**, 163-178 (2006).

50 Titov, V. V. Habitat conditions for *Camelus knoblochi* and factors in its extinction. *Quaternary International* **179**, 120-125, doi:10.1016/j.quaint.2007.10.022 (2008).

51 Mendoza, M., Janis, C. M. & Palmqvist, P. Estimating the body mass of extinct ungulates: a study on the use of multiple regression. *Journal of Zoology* **270**, 90-101, doi:10.1111/j.1469-7998.2006.00094.x (2006).

52 Balco, G., Stone, J. O., Lifton, N. A. & Dunai, T. J. A complete and easily accessible means of calculating surface exposure ages or erosion rates from ^{10}Be and ^{26}Al measurements. *Quaternary Geochronology* **3**, 174-195, doi:10.1016/j.quageo.2007.12.001 (2008).

53 Lal, D. Cosmic ray labeling of erosion surfaces: in situ nuclide production rates and erosion models. *Earth and Planetary Science Letters* **104**, 424-439, doi:10.1016/0012-821x(91)90220-c (1991).

54 Stone, J. O. Air pressure and cosmogenic isotope production. *Journal of Geophysical Research-Solid Earth* **105**, 23753-23759, doi:10.1029/2000jb900181 (2000).

55 Barlow, R. *Barlow, R. Asymmetric Statistical Errors. arXiv physics/0406120 1 (2004), http://www.slac.stanford.edu/~barlow/java/statistics5.html*, 2004).

56 Buckley, M. & Collins, M. J. Collagen survival and its use for species identification in Holocene-lower Pleistocene bone fragments from British archaeological and paleontological sites. *Antiqua* **1**, 1-7 (2011).

57 Buckley, M., Larkin, N. & Collins, M. Mammoth and Mastodon collagen sequences; survival and utility. *Geochimica et Cosmochimica Acta* **75**, 2007-2016, doi:10.1016/j.gca.2011.01.022 (2011).

58 Buckley, M. *et al.* Distinguishing between archaeological sheep and goat bones using a single collagen peptide. *Journal of Archaeological Science* **37**, 13-20, doi:10.1016/j.jas.2009.08.020 (2010).